

Phase locking of a semiconductor double-quantum-dot single-atom maser

Y.-Y. Liu, T. R. Hartke, J. Stehlik, and J. R. Petta

Department of Physics, Princeton University, Princeton, New Jersey 08544, USA

(Received 24 July 2017; published 8 November 2017)

We experimentally study the phase stabilization of a semiconductor double-quantum-dot (DQD) single-atom maser by injection locking. A voltage-biased DQD serves as an electrically tunable microwave frequency gain medium. The statistics of the maser output field demonstrate that the maser can be phase locked to an external cavity drive, with a resulting phase noise $\mathcal{L} = -99$ dBc/Hz at a frequency offset of 1.3 MHz. The injection locking range, and the phase of the maser output relative to the injection locking input tone are in good agreement with Adler's theory. Furthermore, the electrically tunable DQD energy level structure allows us to rapidly switch the gain medium on and off, resulting in an emission spectrum that resembles a frequency comb. The free running frequency comb linewidth is ≈ 8 kHz and can be improved to less than 1 Hz by operating the comb in the injection locked regime.

DOI: [10.1103/PhysRevA.96.053816](https://doi.org/10.1103/PhysRevA.96.053816)

I. INTRODUCTION

Narrow linewidth lasers have a wide range of applications in communication technology, industrial manufacturing, and metrology [1–3]. Unlike in atomic systems, where linewidths can approach 1 mHz [4–6], charge noise in semiconductor lasers typically leads to linewidths that are 10–100 times larger than the Schawlow and Townes (ST) prediction [7–12]. It is therefore often desirable to stabilize the frequency of solid-state masers and lasers using existing narrow linewidth sources via the injection locking effect [13,14]. To achieve an injection-locked state, an external cavity drive is applied to the laser, resulting in stimulated emission at the frequency of the injected signal and a corresponding reduction in linewidth [15]. In addition to frequency stabilization, the precisely locked phase can be used as a resource for other metrology applications. For example, the phase of an injection-locked, trapped-ion-phonon laser has been proposed for applications in mass spectrometry and as an atomic-scale force probe [16].

In this paper we examine phase locking of a DQD semiconductor single-atom maser (SeSAM) [17]. Driven by single electron tunneling events between discrete zero-dimensional electronic states, this device results in microwave frequency photon emission with a free-running emission linewidth of 6 kHz. Due to low frequency charge noise, the linewidth is still 50 times larger than the ST limit [7,9,17,18]. Here we use injection locking to significantly improve the performance of the SeSAM. In contrast with our previous work, which demonstrated injection locking of a multiemitter maser in the frequency regime, the improvement in the emission of the SeSAM allows us to directly measure the degree of phase stabilization in the injection locked state by examining the photon statistics of the output field [19]. The locked maser output achieves a phase noise better than $\mathcal{L} = -99$ dBc/Hz (1.3 MHz offset). The locking phase and locking range are shown to be in good agreement with Adler's prediction [15].

Looking beyond single-tone narrow linewidth sources, the electrically tunable energy level structure of the SeSAM allows the gain medium to be switched on and off. We explore the output of the SeSAM in both free running and injection locked modes while the DQD energy levels are periodically modulated at frequency f_ϵ [20]. When the SeSAM is unlocked, it outputs a frequency comb with a

mode spacing of f_ϵ and an 8-kHz linewidth. Under injection locking conditions, the linewidth of the modulated SeSAM frequency comb emission peaks is reduced to less than 1 Hz, potentially enabling multiplexed readout of superconducting resonator arrays [21,22]. These measurements demonstrate that a single cavity-coupled DQD may serve as a compact, low-temperature microwave source that is suitable for use in quantum computing experiments.

II. DOUBLE-QUANTUM-DOT MICROMASER

The SeSAM is implemented in the circuit quantum electrodynamics architecture (cQED), where strong coupling has been demonstrated between microwave photons and a variety of mesoscopic devices [23–26]. As illustrated in Fig. 1(a), the maser consists of a single semiconductor DQD that is coupled to a microwave cavity [17]. The DQD gain medium is formed from a single InAs nanowire that is bottom gated to create an electrically tunable double-well confinement potential [27,28]. The DQD energy level detuning ϵ is gate-voltage-controlled and a source-drain bias V_{SD} can be applied across the device to result in sequential single electron tunneling. DQD fabrication and characterization details have been described previously [17,18,29].

The cavity consists of a half-wavelength ($\lambda/2$) Nb coplanar waveguide resonator with a resonance frequency $f_c = 7596$ MHz and quality factor $Q_c = 4300$ [17,23,30]. Cavity input and output ports (with designed coupling rates $\kappa_{in}/2\pi = 0.04$ MHz and $\kappa_{out}/2\pi = 0.8$ MHz) are used to drive the SeSAM with the injection locking tone and to measure the internal field of the maser. The cavity output field is amplified and then characterized using either a spectrum analyzer (R&S FSV) or heterodyne detection. With heterodyne detection, the output field is demodulated by a local reference tone of frequency f_{lo} to yield the in-phase (I) and quadrature-phase (Q) components [19,30]. When the cavity is driven by an injection locking tone, the local reference is always set to the injection locking tone frequency $f_{lo} = f_{in}$ in order to measure the phase ϕ of the maser output field relative to the injection locking input tone.

With $V_{SD} = 2$ mV applied, single electron tunneling is allowed when $\epsilon > 0$. In this configuration a single electron

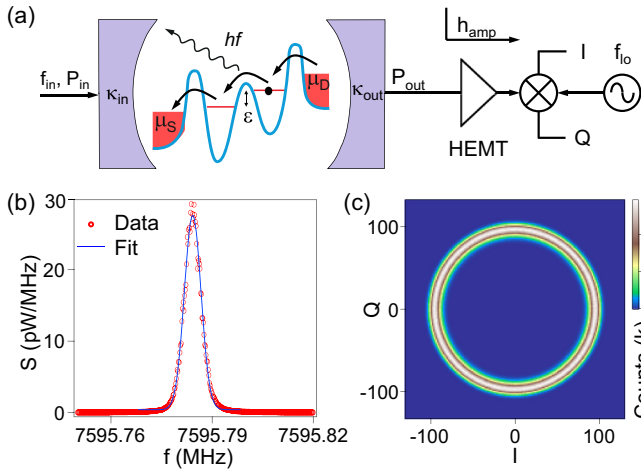


FIG. 1. (a) Schematic of the experimental setup. The SeSAM consists of a DQD gain medium that is placed in a superconducting cavity. A source-drain bias voltage V_{SD} is applied to drive a current through the DQD and generate the microwave frequency photons that result in masing. (b) Free running ($P_{in} = 0$) power spectral density $S(f)$ of the maser output field. The data (circles) are fit with a Gaussian (solid line) with a FWHM $\Gamma = 5.6$ kHz. (c) IQ histogram of the maser output field measured with $P_{in} = 0$. The donut shape is indicative of above-threshold maser action.

tunnels down in energy through the device [see Fig. 1(a)]. The large source-drain bias repumps the DQD excited state and generates the population inversion that is necessary for photon gain in the cavity [17, 18]. A trapped charge in the DQD forms an electric dipole moment that interacts with the cavity field with a rate $g_c/2\pi \approx 70$ MHz [30–35]. Inelastic interdot tunneling results in a combination of phonon and photon emission [18, 28, 36]. The gain mechanism of the SeSAM is similar to the single emitter limit of a quantum cascade laser, where a macroscopic number of electrons flow through quantum well layers and lead to cascaded photon emission [37].

The maser is first characterized in free-running mode with $P_{in} = 0$ (no injection locking tone applied). Figure 1(b) plots the power spectral density of the output radiation $S(f)$. The emission peak is nicely fit by a Gaussian with a FWHM $\Gamma = 5.6$ kHz that is 300 times narrower than the cavity linewidth $\kappa_{tot}/2\pi = f_c/Q_c = 1.8$ MHz. The emission signal, and its narrow linewidth, are suggestive of an above-threshold maser state. Maser action is confirmed by measuring the statistics of the output field [17, 18]. Figure 1(c) shows the two-dimensional histogram resulting from 1.7×10^7 individual (I, Q) measurements that were sampled at a rate of 12.3 MHz. Here $f_{io} = f_e = 7595.8$ MHz, where f_e is the emission frequency. The IQ histogram has donut shape that is consistent with an above-threshold maser.

Compared to the two-emitter maser investigated in our previous work [19], the SeSAM has more stable emission properties. The emission linewidth has been reduced from 34 kHz to 5.6 kHz, and fewer “blinking events” (where the maser emission turns off) are observed in the IQ histogram. However, the histogram clearly shows that the phase of the maser output samples all angles in the (I, Q) plane, which indicates there are large phase fluctuations in free

running mode. The randomization of phase is attributed to low frequency ($1/f$) charge noise that is induced by charged two-level systems on the surface of the nanowire or near the nanowire. Previous experiments indicate that the detuning noise has an amplitude of approximately $5 \mu\text{eV}$ [19, 33]. In this paper we use injection locking to further improve the output characteristics of the SeSAM.

III. INJECTION LOCKING RESULTS

The improvement in the maser emission of the SeSAM relative to previous two-emitter devices enables a more careful investigation of the degree to which the output characteristics of the SeSAM can be improved using injection locking. In Sec. III A we present results showing that the maser emission can be phase locked by driving the input port of the cavity with an injection locking tone. In the injection locked state, the maser output field has a phase noise $\mathcal{L} = -99$ dBc/Hz at $f_e = 7595.8$ MHz (1.3 MHz offset). In Sec. III B, we measure the phase of the maser output field relative to the injection locking input tone as a function of input frequency, and show that it is in good agreement with Adler’s prediction. We then measure the injection locking range as a function of injection locking input tone power in Sec. III C. The phase and frequency locking range measurements are consistent with each other, giving further evidence that the frequency locking observed in previous work is due to phase stabilization via the injection locking effect [19].

A. Phase locking the SeSAM

We first demonstrate frequency narrowing of the maser emission relative to the free-running state using injection locking [19]. Figure 2(a) shows $S(f)$ as a function of the injection locking input tone power P_{in} with $f_{in} = 7595.805$ MHz set near the free running emission frequency f_e for this device tuning configuration. For negligible input powers ($P_{in} < -125$ dBm) the emission spectrum exhibits a broad peak near 7595.805 MHz with a typical FWHM $\Gamma \approx 6$ kHz. Due to low frequency charge noise, the center frequency of the free-running emission peak fluctuates within the range $f_e = 7595.805 \pm 0.005$ MHz. With $P_{in} > -125$ dBm, the broad tails of the emission peak are suppressed and the spectrum begins to narrow. The SeSAM eventually locks to the injection locking input tone around $P_{in} = -115$ dBm. In the injection locked state, the large fluctuations in f_e are suppressed and the measured linewidth is $\Gamma \approx 100$ Hz, more than a factor of 50 narrower than the free-running case [38].

The IQ histograms in Figs. 2(b)–2(h) demonstrate the evolution of the maser output phase relative to the injection locking input tone as P_{in} is increased (for these data sets $f_{io} = f_{in}$). A movie showing the evolution with P_{in} is included in the Supplemental Material [39]. For small $P_{in} < -120$ dBm, the histograms shown in Figs. 2(b)–2(d) have a ring shape. In contrast to the free-running histogram shown in Fig. 1(c), these histograms have an unequal weighting in the IQ plane. For example, the Fig. 2(d) histogram has a higher count density for phase angles around $\phi = -30^\circ$. The ring shape indicates that the relative phase of the injection locking input tone and

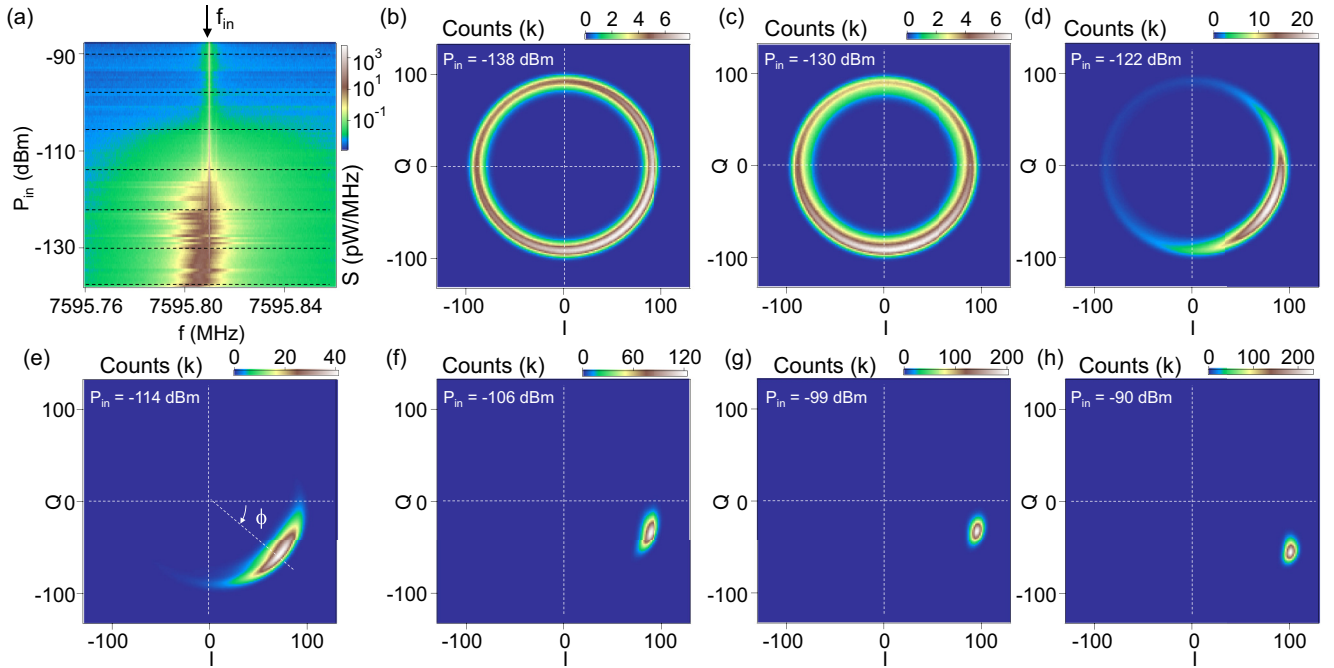


FIG. 2. (a) Emission power spectral density $S(f)$ as a function of P_{in} . The injection locking tone input frequency $f_{\text{in}} = 7595.805$ MHz is set to be close to the free running maser emission frequency $f_e = 7595.805 \pm 0.005$ MHz. Note the significant fluctuations in f_e for $P_{\text{in}} < -125$ dBm. The maser linewidth narrows with increasing P_{in} due to injection locking. (b)–(d) For $P_{\text{in}} < -115$ dBm, the cavity field is a combination of the free running maser emission and the cavity input tone at f_{in} . In this configuration the maser is unlocked and its phase fluctuates relative to the injection locking input tone. Here the IQ histograms have population in all 360° degrees of the IQ plane. (e)–(h) For larger $P_{\text{in}} > -115$ dBm, the maser is phase locked to the input tone, and the phase distribution is further narrowed with increasing P_{in} .

the maser emission are unlocked, while the increased number of counts near a specific phase angle ϕ is due to stimulated emission at f_{in} . The radius of the rings in the IQ plane doesn't significantly change as P_{in} is increased, which indicates that the total output power of the SeSAM is nearly constant and limited by the DQD photon emission rate. As P_{in} is further increased, the phase distribution continues to narrow, consistent with the narrowing of the emission peak shown in Fig. 2(a) [19].

Around $P_{\text{in}} = -115$ dBm the ring-shaped IQ histogram evolves into a distribution that is localized within a relative phase $\phi \pm \Delta\phi = \phi \pm 3\sigma_{\phi,h} = -40 \pm 60^\circ$, as demonstrated in Fig. 2(e). Here $\phi = \arctan(\bar{I}, \bar{Q})$ is the maximally populated angle and $\sigma_{\phi,h}$ is the measured standard deviation. In this configuration the phase of the maser output is locked to the injection locking input tone. The distribution in phase space is further narrowed with increasing P_{in} as demonstrated by Figs. 2(f)–2(h), where the relative phase is $\phi = -20 \pm 12^\circ$ for $P_{\text{in}} > -100$ dBm. The P_{in} value at which phase stabilization occurs is in good agreement with the value of P_{in} where frequency locking occurs, as demonstrated in Fig. 2(a).

The detected phase fluctuations in the histograms have a standard deviation $\sigma_{\phi,h} = 4^\circ$ for $P_{\text{in}} > -100$ dBm. These fluctuations have a contribution from the intrinsic maser output fluctuations with a standard deviation $\sigma_{\phi,0}$ and a contribution from amplifier background noise h_{amp} [see Fig. 1(a)], which has $\langle h_{\text{amp}}^\dagger h_{\text{amp}} \rangle = 42$ [18,30,40]. The detected field $\alpha = I + iQ$ consists of $\alpha = \alpha_0 + h_{\text{amp}}$, where $\alpha_0 = I_0 + iQ_0$ is the cavity output. Given α_0 is independent of h_{amp} and $\langle h_{\text{amp}} \rangle = 0$, the distribution in the detected phase

$\phi_h = \arg(\alpha) = \arctan(I, Q)$ (in units of rad) has a standard deviation,

$$\sigma_{\phi,h}^2 = \sigma_{\phi,0}^2 + \langle h_{\text{amp}}^\dagger h_{\text{amp}} \rangle / \langle I^2 + Q^2 \rangle.$$

After subtracting h_{amp} , the maser output phase fluctuations have a standard deviation $\sigma_{\phi,0} = 1.5^\circ$ within our detection resolution bandwidth $\text{RBW} = 2.6$ MHz. The average phase noise of the locked maser output near f_e is then estimated to be $\mathcal{L} = \sigma_{\phi,0}^2 / 2\text{RBW} = 1.3 \times 10^{-10}$ rad²/Hz or, equivalently, $\mathcal{L} = -99$ dBc/Hz at a frequency offset of 1.3 MHz, when $P_{\text{in}} > -100$ dBm. For comparison, the phase noise is 40–50 dBc/Hz larger than a typical precision microwave source such as the Keysight E8267D.

B. Phase evolution across the injection locking range

We now investigate the relative phase ϕ between the maser output and the injection locking input tone across the full injection locking range. The insets of Fig. 3 show IQ histograms acquired with $P_{\text{in}} = -98$ dBm at $f_{\text{in}} = 7595.64$ MHz (left inset) and $f_{\text{in}} = 7595.73$ MHz (right inset). With $f_{\text{in}} = 7595.64$ MHz, which is detuned by 0.17 MHz from the free-running maser frequency $f_e = 7595.81$, the IQ distribution has a ringlike shape and thus the phase is unlocked. Note that in this regime the output is essentially the sum of two different tones, and this results in a noticeable offset in the ring. When f_{in} approaches f_e , the phase will be localized within a small range, as demonstrated in the right inset, which

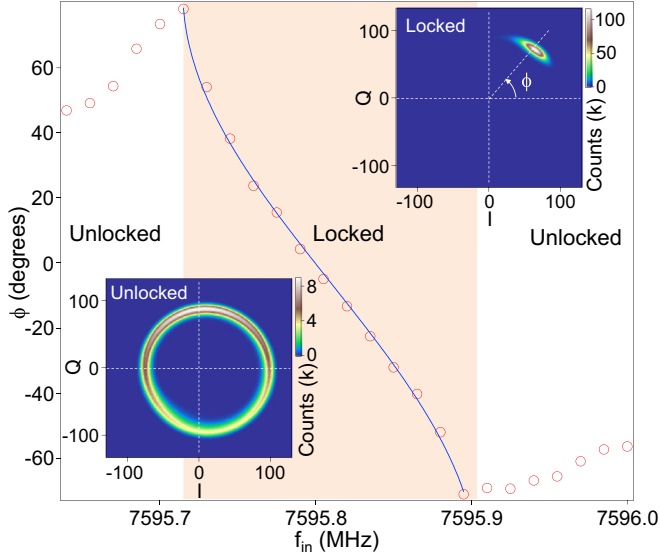


FIG. 3. The phase ϕ of the maser emission relative to the injection locking input tone as a function of f_{in} at $P_{\text{in}} = -98$ dBm. The blue curve is the prediction from Adler's theory. (Left inset) IQ histogram of the output field with $f_{\text{in}} = 7595.64$ MHz, where the emission phase is unlocked. (Right inset) IQ histogram of the maser output field at $f_{\text{in}} = 7595.73$ MHz, where the phase of the maser is locked to the injection locking input tone with $\phi = 48^\circ$.

shows a distribution that is limited to $\phi = 48 \pm 15^\circ$. Here f_{in} is detuned from f_e by only 0.08 MHz.

The main panel of Fig. 3 shows ϕ as a function of f_{in} with $P_{\text{in}} = -98$ dBm. Within the indicated frequency range of $\Delta f_{\text{in}} = 0.19$ MHz, the histograms are similar to the right inset and show output phases in the range $\phi \in (-90^\circ, 90^\circ)$. The maser output is thus “phase locked” to the input tone when $|f_{\text{in}} - f_e|$ is small.

The measured phase can be compared with predictions from Adler's theory, which analyzes the maser dynamics when the injection locking tone input power is small compared to the free-running emission power [15]. We express the cavity output field in the laboratory frame as

$$\alpha(t) = I(t) + iQ(t) = \sqrt{\frac{P_{\text{out}}}{\text{RBW} h f_e}} e^{2\pi i f_{\text{in}} t + i\phi(t)}, \quad (1)$$

where P_{out} is the output power. The relative phase follows the Adler equation:

$$\frac{d\phi}{dt} + 2\pi(f_{\text{in}} - f_e) = -2\pi \frac{\Delta f_{\text{in}}}{2} \sin(\phi). \quad (2)$$

In the injection locking range $|f_{\text{in}} - f_e| < \Delta f_{\text{in}}/2$, Eq. (2) has a static solution,

$$\phi = \arcsin[2(f_e - f_{\text{in}})/\Delta f_{\text{in}}]. \quad (3)$$

Fluctuations in ϕ can be introduced by fluctuations in f_e and the intrinsic standard deviation $\sigma_{\phi,0}$ diverges near the boundaries of the injection locking range. Outside of this range ϕ is unlocked. The phase dependence predicted by the Adler equation is plotted as the blue curve in Fig. 3 and is in good agreement with our data.

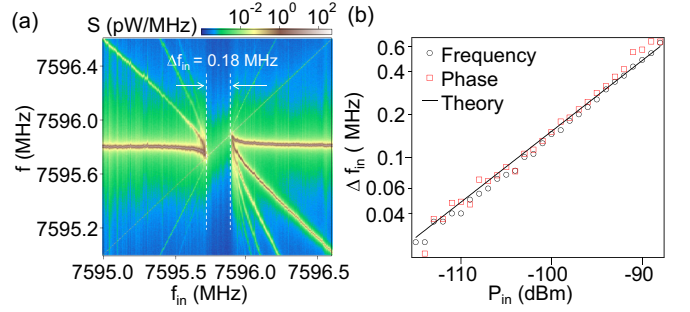


FIG. 4. (a) $S(f)$ measured as a function of f_{in} with $P_{\text{in}} = -98$ dBm. The white dashed lines indicate the injection locking range Δf_{in} . (b) Δf_{in} as a function of P_{in} . The locking range is extracted from measurements of $S(f)$ (circles) and from the phase locking range in the IQ histograms (squares). The black line is a fit to the power law $\Delta f_{\text{in}} \propto \sqrt{P_{\text{in}}}$ prediction of the Adler equation.

C. Injection locking range

We next determine the frequency locking range from measurements of $S(f)$ and compare these data with the phase locking measurements presented in the previous section. Figure 4(a) shows a color-scale plot of $S(f)$ as a function of f_{in} measured with $P_{\text{in}} = -98$ dBm. Similar to our previous work, frequency pulling is visible and emission sidebands appear as a mixing between the injection locking input tone and the free-running maser emission when f_{in} approaches f_e [19,41,42]. The maser then abruptly locks to f_{in} , and remains locked to f_{in} over a frequency range $\Delta f_{\text{in}} = 0.18$ MHz. The frequency locking range is consistent with the phase locking data shown in Fig. 3, which is measured at the same P_{in} .

By repeating these measurements at different P_{in} , we obtain the data shown in Fig. 4(b), where Δf_{in} measured by the two methods is plotted as a function of P_{in} . The measurements are in good agreement, verifying that the frequency locking we observe in measurements of $S(f)$ is due to the injection locking effect [19]. The black line in Fig. 4(b) is a fit to the power law relation $\Delta f_{\text{in}} = A_M \sqrt{P_{\text{in}}}$, with the measured prefactor $A_M = (0.48 \pm 0.16) \times 10^6$ MHz/ $\sqrt{\text{W}}$, where the error bar is due to the uncertainty in the input transmission line losses. From theory, we find

$$A_T = \frac{C_\kappa}{\sqrt{P_{\text{out}}}} \frac{\kappa_{\text{tot}}}{2\pi} = (0.87 \pm 0.29) \times 10^6 \text{ MHz}/\sqrt{\text{W}},$$

where the cavity prefactor $C_\kappa = 2\sqrt{\kappa_{\text{in}}\kappa_{\text{out}}}/\kappa_{\text{tot}}$ accounts for internal cavity losses and is obtained using cavity input-output theory [19,41]. The error bar is due to the uncertainty in $\kappa_{\text{in}/\text{out}}$ and the calibration of P_{out} . We therefore find reasonable agreement between the data and the predictions from Adler's theory, considering the uncertainties in the transmission line losses.

IV. MICROWAVE FREQUENCY COMB

We have so far examined the output characteristics of the SeSAM in free-running mode and under the influence of an injection locking tone. In this section, we investigate the output characteristics of the SeSAM while a periodic modulation is applied to the DQD energy levels, which modulates the gain medium. With the periodic modulation applied, we observe

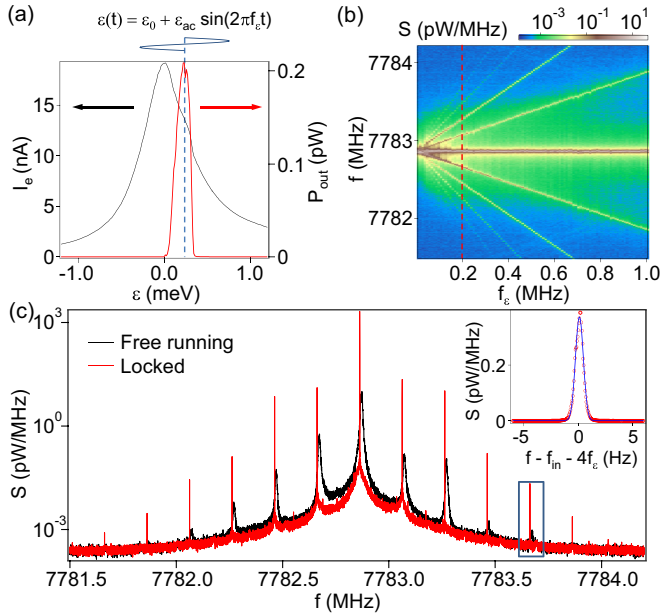


FIG. 5. (a) I_e (black) and P_{out} (red) plotted as a function of ϵ . A sinusoidal drive is applied to the detuning parameter to modulate the gain of the DQD maser. (b) $S(f)$ as a function of f_ϵ with $\epsilon_{ac} = 0.2$ meV and $P_{in} = 0$. A frequency comb is observed with the spacing set by f_ϵ . (c) $S(f)$ with $f_\epsilon = 0.2$ MHz and $\epsilon_{ac} = 0.2$ meV. The black curve is the frequency comb measured in free-running mode with $P_{in} = 0$. The red curve is the frequency comb acquired under injection locking conditions with $f_{in} = 7782.9$ MHz and $P_{in} = -108$ dBm. (Inset) A zoom-in of the injection locked comb at the fourth sideband.

a comblike emission spectrum, where the spacing between the emission peaks is set by the modulation frequency. The SeSAM frequency comb can also be operated under injection locking conditions, which leads to a dramatic narrowing of the emission peaks. The data presented in this section were acquired on a different device that has an emission frequency $f_c = 7782.86$ MHz and linewidth $\Gamma = 3$ kHz.

The modulation method is described in Fig. 5(a), which plots the electron current I_e and P_{out} as a function of ϵ . In free-running mode, the maximum output power $P_{out} = 0.2$ pW is obtained at an offset detuning $\epsilon_0 = 0.2$ meV due to a strong phonon sideband [43]. We next modulate the gain medium by applying a sine wave to the DQD gates, such that $\epsilon = \epsilon_0 + \epsilon_{ac} \sin(2\pi f_\epsilon t)$. Here ϵ_{ac} and f_ϵ are the amplitude and frequency of the detuning modulation. As shown in Fig. 5(a), the SeSAM emission power is strongly detuning dependent. Therefore the effective gain rate will be modulated by the sinusoidal gate drive [18].

Figure 5(b) plots $S(f)$ as a function of f_ϵ with $\epsilon_{ac} = 0.2$ meV. We observe a central emission peak around $f = 7782.86$ MHz that is independent of f_ϵ . In addition to the central emission peak we observe a series of narrow emission peaks that shift away from the central emission peak as f_ϵ is increased. Up to four emission sidebands are clearly observed on both the low and high frequency sides of the central emission peak. With such a large modulation amplitude

applied, photoemission from the DQD will turn on and off at a beat frequency f_ϵ . The beating in the time domain results in sidebands in the frequency domain, with a sideband spacing set by f_ϵ . The black curve in Fig. 5(c) shows a line cut through the data in Fig. 5(b) at $f_\epsilon = 0.2$ MHz. The sidebands can be fit to a Lorentzian with a linewidth of 8 kHz, similar to the free-running maser linewidth $\Gamma = 3$ kHz. Similar, but weaker comb sidebands are also observed with a smaller ϵ_{ac} .

The linewidth of the emission peaks in the frequency comb can be significantly improved using the injection locking effect [3]. For example, the red curve in Fig. 5(c) shows $S(f)$ when the frequency comb is injection locked to an input tone at $f_{in} = 7782.86$ MHz and $P_{in} = -108$ dBm. Compared to the free-running frequency comb data, the peak height and linewidth of the injection locked frequency comb have been dramatically improved. In addition, we observe two additional sidebands on both the low and high frequency sides of the central emission peak. The inset of Fig. 5(c) shows $S(f)$ measured near the fourth sideband on the high frequency side of the central emission peak [near $f = 7783.65$ MHz, see rectangle in main panel of Fig. 5(c)]. The sideband is best fit to a Gaussian of width 0.9 Hz, which is most likely limited by the 1-Hz resolution bandwidth of the microwave frequency spectrum analyzer [38].

V. CONCLUSION AND OUTLOOK

We have presented experimental evidence of phase locking of a semiconductor DQD single-atom maser (SeSAM). The statistics of the maser emission in the complex plane demonstrates that the SeSAM can be phase locked to an injection locking input tone resulting in an emission signal with a phase noise $\mathcal{L} = -99$ dBc/Hz at a frequency offset of 1.3 MHz. Both phase and frequency locking data are shown to be in good agreement with Adler's prediction. In addition, we utilize the electrical tunability of the DQD energy level structure to modulate the DQD gain medium. The resulting emission spectrum is a frequency comb, where individual emission peaks in the comb have a linewidth of around 8 kHz. By injection locking the SeSAM, we reach linewidths < 1 Hz, an 8000-fold improvement. The SeSAM allows for studies of fundamental light-matter interactions in condensed matter systems. These measurements demonstrate that a single DQD may serve as a compact low-temperature microwave source that is suitable for use in quantum computing experiments.

ACKNOWLEDGMENTS

We thank M. J. Gullans and J. M. Taylor for helpful discussions and acknowledge support from the Packard Foundation, the National Science Foundation Grant No. DMR-1409556, and the Gordon and Betty Moore Foundation's EPiQS Initiative through Grant No. GBMF4535. Devices were fabricated in the Princeton University Quantum Device Nanofabrication Laboratory.

- [1] D. Kleppner, H. M. Goldenberg, and N. F. Ramsey, Properties of the hydrogen maser, *Appl. Opt.* **1**, 55 (1962).
- [2] D. Kleppner, H. C. Berg, S. B. Crampton, N. F. Ramsey, R. F. C. Vessot, H. E. Peters, and J. Vanier, Hydrogen-maser principles and techniques, *Phys. Rev.* **138**, A972 (1965).
- [3] S. A. Diddams, D. J. Jones, J. Ye, S. T. Cundiff, J. L. Hall, J. K. Ranka, R. S. Windeler, R. Holzwarth, T. Udem, and T. W. Hänsch, Direct Link between Microwave and Optical Frequencies with a 300 THz Femtosecond Laser Comb, *Phys. Rev. Lett.* **84**, 5102 (2000).
- [4] D. Meiser, J. Ye, D. R. Carlson, and M. J. Holland, Prospects for a Millihertz-Linewidth Laser, *Phys. Rev. Lett.* **102**, 163601 (2009).
- [5] T. Kessler, C. Hagemann, C. Grebing, T. Legero, U. Sterr, F. Riehle, M. J. Martin, L. Chen, and J. Ye, A sub-40-mHz-linewidth laser based on a silicon single-crystal optical cavity, *Nat. Photon.* **6**, 687 (2012).
- [6] J. G. Bohnet, Z. Chen, J. M. Weiner, D. Meiser, M. J. Holland, and J. K. Thompson, A steady-state superradiant laser with less than one intracavity photon, *Nature (London)* **484**, 78 (2012).
- [7] A. L. Schawlow and C. H. Townes, Infrared and optical masers, *Phys. Rev.* **112**, 1940 (1958).
- [8] A. E. Siegman, *Microwave Solid-State Masers* (McGraw-Hill, New York, 1964).
- [9] P. W. Milonni and J. H. Eberly, *Lasers* (Wiley, New York, 1988).
- [10] G. Dick and R. Wang, Ultra-Stable Performance of the Superconducting Cavity Maser, *IEEE Trans. Instrum. Meas.* **40**, 174 (1991).
- [11] P.-Y. Bourgeois, N. Bazin, Y. Kersal, V. Giordano, M. E. Tobar, and M. Oxborrow, Maser oscillation in a whispering-gallery-mode microwave resonator, *Appl. Phys. Lett.* **87**, 224104 (2005).
- [12] M. Oxborrow, J. D. Breeze, and N. M. Alford, Room-temperature solid-state maser, *Nature (London)* **488**, 353 (2012).
- [13] H. L. Stover and W. H. Steier, Locking of laser oscillation by light injection, *Appl. Phys. Lett.* **8**, 91 (1966).
- [14] U. Schünemann, H. Engler, M. Zielonkowski, M. Weidemüller, and R. Grimm, Magneto-optic trapping of lithium using semiconductor lasers, *Opt. Commun.* **158**, 263 (1998).
- [15] R. Adler, A study of locking phenomena in oscillators, *Proc. IRE* **34**, 351 (1946).
- [16] S. Knünz, M. Herrmann, V. Batteiger, G. Saathoff, T. W. Hänsch, K. Vahala, and T. Udem, Injection Locking of a Trapped-Ion Phonon Laser, *Phys. Rev. Lett.* **105**, 013004 (2010).
- [17] Y.-Y. Liu, J. Stehlik, C. Eichler, X. Mi, T. R. Hartke, M. J. Gullans, J. M. Taylor, and J. R. Petta, Threshold Dynamics of a Semiconductor Single Atom Maser, *Phys. Rev. Lett.* **119**, 097702 (2017).
- [18] Y.-Y. Liu, J. Stehlik, C. Eichler, M. J. Gullans, J. M. Taylor, and J. R. Petta, Semiconductor double quantum dot micromaser, *Science* **347**, 285 (2015).
- [19] Y.-Y. Liu, J. Stehlik, M. J. Gullans, J. M. Taylor, and J. R. Petta, Injection locking of a semiconductor double-quantum-dot micromaser, *Phys. Rev. A* **92**, 053802 (2015).
- [20] M. C. Cassidy, A. Bruno, S. Rubbert, M. Irfan, J. Kammhuber, R. N. Schouten, A. R. Akhmerov, and L. P. Kouwenhoven, Demonstration of an ac Josephson junction laser, *Science* **355**, 939 (2017).
- [21] S. McHugh, B. A. Mazin, B. Serfass, S. Meeker, K. O'Brien, R. Duan, R. Raffanti, and D. Werthimer, A readout for large arrays of microwave kinetic inductance detectors, *Rev. Sci. Instrum.* **83**, 044702 (2012).
- [22] O. Noroozian, P. K. Day, B. H. Eom, H. G. Leduc, and J. Zmuidzinas, Crosstalk Reduction for Superconducting Microwave Resonator Arrays, *IEEE Trans. Microwave Theory Tech.* **60**, 1235 (2012).
- [23] A. Wallraff, D. I. Schuster, A. Blais, L. Frunzio, R.-S. Huang, J. Majer, S. Kumar, S. M. Girvin, and R. J. Schoelkopf, Strong coupling of a single photon to a superconducting qubit using circuit quantum electrodynamics, *Nature (London)* **431**, 162 (2004).
- [24] X. Mi, J. V. Cady, D. M. Zajac, P. W. Deelman, and J. R. Petta, Strong coupling of a single electron in silicon to a microwave photon, *Science* **355**, 156 (2017).
- [25] A. Stockklauser, P. Scarlino, J. V. Koski, S. Gasparinetti, C. K. Andersen, C. Reichl, W. Wegscheider, T. Ihn, K. Ensslin, and A. Wallraff, Strong Coupling Cavity QED with Gate-Defined Double Quantum Dots Enabled by a High Impedance Resonator, *Phys. Rev. X* **7**, 011030 (2017).
- [26] L. E. Bruhat, T. Cubaynes, J. J. Viennot, M. C. Dartailh, M. M. Desjardins, A. Cottet, and T. Kontos, Strong Coupling Between an Electron in a Quantum Dot Circuit and a Photon in a Cavity, [arXiv:1612.05214](https://arxiv.org/abs/1612.05214).
- [27] S. Nadj-Perge, S. M. Frolov, E. P. A. M. Bakkers, and L. P. Kouwenhoven, Spin-orbit qubit in a semiconductor nanowire, *Nature (London)* **468**, 1084 (2010).
- [28] W. G. van der Wiel, S. De Franceschi, J. M. Elzerman, T. Fujisawa, S. Tarucha, and L. P. Kouwenhoven, Electron transport through double quantum dots, *Rev. Mod. Phys.* **75**, 1 (2002).
- [29] Y.-Y. Liu, K. D. Petersson, J. Stehlik, J. M. Taylor, and J. R. Petta, Photon Emission from a Cavity-Coupled Double Quantum Dot, *Phys. Rev. Lett.* **113**, 036801 (2014).
- [30] J. Stehlik, Y.-Y. Liu, C. Eichler, T. R. Hartke, X. Mi, M. J. Gullans, J. M. Taylor, and J. R. Petta, Double Quantum Dot Floquet Gain Medium, *Phys. Rev. X* **6**, 041027 (2016).
- [31] M. R. Delbecq, V. Schmitt, F. D. Parmentier, N. Roch, J. J. Viennot, G. Fève, B. Huard, C. Mora, A. Cottet, and T. Kontos, Coupling a Quantum Dot, Fermionic Leads, and a Microwave Cavity on a Chip, *Phys. Rev. Lett.* **107**, 256804 (2011).
- [32] T. Frey, P. J. Leek, M. Beck, A. Blais, T. Ihn, K. Ensslin, and A. Wallraff, Dipole Coupling of a Double Quantum Dot to a Microwave Resonator, *Phys. Rev. Lett.* **108**, 046807 (2012).
- [33] K. D. Petersson, L. W. McFaul, M. D. Schroer, M. Jung, J. M. Taylor, A. A. Houck, and J. R. Petta, Circuit quantum electrodynamics with a spin qubit, *Nature (London)* **490**, 380 (2012).
- [34] M. R. Delbecq, L. E. Bruhat, J. J. Viennot, S. Datta, A. Cottet, and T. Kontos, Photon-mediated interaction between distant quantum dot circuits, *Nat. Commun.* **4**, 1400 (2013).
- [35] H. Toida, T. Nakajima, and S. Komiyama, Vacuum Rabi Splitting in a Semiconductor Circuit QED System, *Phys. Rev. Lett.* **110**, 066802 (2013).
- [36] T. Fujisawa, T. H. Oosterkamp, W. G. van der Wiel, B. W. Broer, R. Aguado, S. Tarucha, and L. P. Kouwenhoven, Spontaneous emission spectrum in double quantum dot devices, *Science* **282**, 932 (1998).
- [37] J. Faist, F. Capasso, D. L. Sivco, C. Sirtori, A. L. Hutchinson, and A. Y. Cho, Quantum cascade laser, *Science* **264**, 553 (1994).

- [38] The frequency resolution is limited by the resolution bandwidth of the R&S spectrum analyzer FSV. The selection of the RBW is determined by a balance between better resolution in the locked case and the range of frequency we need to cover in the free-running case. For Fig. 2 the RBW is set to 0.1 kHz, for Fig. 4 the RBW is set to 1 kHz, for Figs. 5(b) and 5(c) main panel the RBW is set to 0.1 kHz, and for Fig. 5(c) inset and Fig. 5(d) the RBW is set to 1 Hz.
- [39] See Supplemental Material at <http://link.aps.org/supplemental/10.1103/PhysRevA.96.053816> for a movie showing the evolution of emission statistics with increasing input power.
- [40] C. Eichler, D. Bozyigit, and A. Wallraff, Characterizing quantum microwave radiation and its entanglement with superconducting qubits using linear detectors, *Phys. Rev. A* **86**, 032106 (2012).
- [41] A. E. Siegman, *Lasers* (University Science Books, Mill Valley, 1986).
- [42] M. Armand, On the output spectrum of unlocked driven oscillators, *Proc. IEEE* **57**, 798 (1969).
- [43] M. J. Gullans, Y.-Y. Liu, J. Stehlik, J. R. Petta, and J. M. Taylor, Phonon-Assisted Gain in a Semiconductor Double Quantum Dot Maser, *Phys. Rev. Lett.* **114**, 196802 (2015).